POROMECHANICS RESPONSE OF AN INCLINED BOREHOLE
SUBJECT TO IN-SITU STRESS AND FINITE LENGTH FLUID
DISCHARGE

Younane N. Abousleiman and Shengli Chen

POROMECHANICS RESPONSE OF AN INCLINED BOREHOLE SUBJECT TO IN-SITU STRESS AND FINITE LENGTH FLUID DISCHARGE

YOUNANE N. ABOUSLEIMAN AND SHENGLI CHEN

The analytical approach developed in this paper calculates the poroelastic coupled time-dependent stress and pore pressure variations for an inclined borehole drilled in a fluid saturated porous medium and subjected to the far-field three-dimensional in-situ stresses in addition to a fluid discharge over a finite length of its surface. This problem is encountered in many engineering applications, in particular, in wellbore drilling, fluid injection, and production. A superposition scheme is employed to obtain the analytical solutions within the linear theory of poromechanics. The comparison with an earlier published solution shows a discrepancy in the poroelastic boundary conditions applied at the wellbore wall. In this solution a systematic analysis is being carried out to evaluate the effects of the mechanical parameters on the calculated time-dependent effective tangential stress and pore pressure in addition to the effects of the borehole inclination and the geometry of the flux loading area are also included.

1. Introduction

The generalized poromechanics solutions of an inclined borehole, which extend the isotropic plane strain solution of Carter and Booker [1982] and the one slightly modified by Detournay and Cheng [1988] to an anisotropic porous medium (coupled with thermal and chemical effects) [Abousleiman and Ekbote 2005; Ekbote and Abousleiman 2005; 2006], have seen many applications in engineering problems, in particular in the oil and gas industry [Abousleiman et al. 1999], where these problems are of great economic value to operations. Lately, these solutions have been extended for estimating stress and pore pressure distributions in a borehole drilled in naturally fractured fluid saturated medium [Abousleiman and Nguyen 2005] following the mixture theory approach in [Bowen 1982].

Poromechanics theory was first established by [Biot 1941] and has served as the basis for many of the later works on borehole problems. Cui et al. [1997; 1998; 1999] presented the analytical solutions for the general case, where the borehole is inclined to the three-dimensional principal axes of the far-field in-situ stresses using a loading decomposition scheme. In an earlier study, Rajapakse [1993] obtained a set of general stress solutions associated with free stress boundaries, yet a fluid source applied over a finite segment of the borehole wall.

For a wide range of engineering applications in the oil and gas industry it has been customary practice to inject fluid into a sealed segment of the borehole at great depth. In reservoir stimulation, hydraulic fracturing is one of the most widely used techniques, it also extends to applications in environmental

engineering for clean ups. In addition, from such geometries an extended leak-off test is commonly performed to estimate the far field in-situ stresses. For these important problems, the poromechanics solution does not exist in the literature. Although Rajapakse [1993] considered the fluid flowing into the finite length of the borehole, and its effects on the stress and pore pressure perturbation, the assumptions were that the formation is initially unstressed and consists of incompressible constituents. Moreover, it was clearly incorrect in his study to claim that the total radial stress be zero over the fluid injection segment of the borehole wall. While in the existing solutions [Cui et al. 1997; 1998; 1999; Abousleiman and Ekbote 2005], efforts were focused upon an infinite length inclined borehole with only stress and pore pressure boundary conditions. Therefore, a more general solution, which could take into account the fluid injection on a finite geometry of the wellbore coupled with the three-dimensional far field in-situ stresses is needed.

The purpose of this paper is to present the analytical stress analysis and pore pressures of an inclined borehole subjected to fluid discharge over a finite segment of the surface and to the three-dimensional in-situ far field state of stress. Based on linear poromechanics and a careful inspection of the boundary conditions, the problem is divided into two fundamental parts, specifically, a fluid discharge problem, and a stress boundary problem. These time-dependent problems are solved using the Laplace and Fourier integral transforms. The final stress solutions thus may be deduced by simple superposition. Comprehensive numerical analyses are carried out in the paper to present comparison with the existing solutions and to investigate the influences of the material properties, borehole inclination, as well as the flux loading area on the calculated effective tangential stress and pore pressure.

2. Governing equations

Consider an inclined borehole with radius R drilled in an infinite porous medium which is characterized by a nonhydrostatic in-situ stress field, see Figure 1a. The borehole is subjected to a radial fluid discharge over a segment of the surface. Using the cylindrical coordinates system (r, θ, z), see Figure 1b, the governing equations for deformations of the isotropic homogeneous saturated medium can be expressed as follows [Biot 1941; Rice and Cleary 1976; Wang 2000]:

$$\nabla^2 u_r + \frac{1}{1-2v_u}\frac{\partial e_v}{\partial r} - \frac{1}{r}\left(\frac{2}{r}\frac{\partial u_\theta}{\partial \theta} + \frac{u_r}{r}\right) - \frac{2B(1+v_u)}{3(1-2v_u)}\frac{\partial \varepsilon_v}{\partial r} = 0, \tag{1}$$
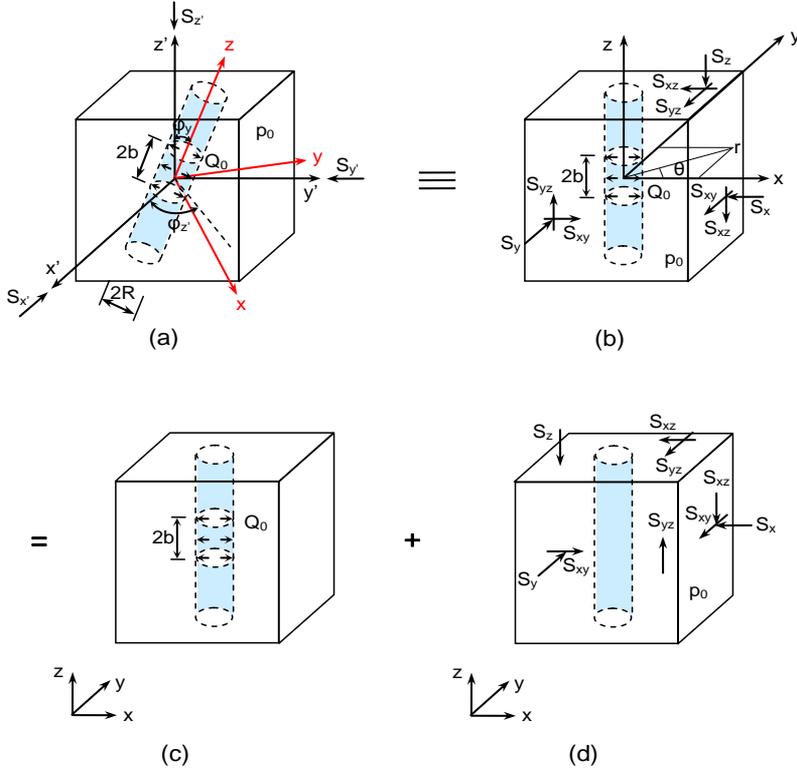
$$\nabla^2 u_\theta + \frac{1}{1-2v_u}\frac{\partial e_v}{r\partial \theta} - \frac{1}{r}\left(\frac{u_\theta}{r} - \frac{2}{r}\frac{\partial u_r}{\partial \theta}\right) - \frac{2B(1+v_u)}{3(1-2v_u)}\frac{\partial \varepsilon_v}{r\partial \theta} = 0, \tag{2}$$

$$\nabla^2 u_z + \frac{1}{1-2v_u}\frac{\partial e_v}{\partial z} - \frac{2B(1+v_u)}{3(1-2v_u)}\frac{\partial \varepsilon_v}{\partial z} = 0, \tag{3}$$

$$\nabla^2 \varepsilon_v = \frac{1}{c}\frac{\partial \varepsilon_v}{\partial t} \tag{4}$$

in which u_r, u_θ, and u_z are radial, circumferential, and vertical displacements of the solid matrix;

$$e_v = \frac{\partial u_r}{\partial r} + \frac{u_r}{r} + \frac{\partial u_\theta}{r\partial \theta} + \frac{\partial u_z}{\partial z}$$

Figure 1. Geometry of inclined borehole and decomposition scheme: (a) borehole inclined to principal stresses; (b) equivalent far field stresses in local coordinate system; (c) fluid discharge problem; (d) stress boundary problem.

is the matrix dilation and ε_v is the variation of fluid content per unit reference volume; B is Skempton pore pressure coefficient;

$$c = \frac{2G\kappa B^2(1-\nu)(1+\nu_u)^2}{9(1-\nu_u)(\nu_u-\nu)}$$

is the diffusion coefficient, G is the shear modulus, ν and ν_u are the drained and undrained Poisson's ratios, and κ is defined by $\kappa = k/\mu$, with k denoting the intrinsic permeability (mD) and μ the fluid viscosity; and ∇^2 denotes the Laplacian operator which is given by

$$\nabla^2 = \frac{\partial^2}{\partial r^2} + \frac{1}{r}\frac{\partial}{\partial r} + \frac{1}{r^2}\frac{\partial^2}{\partial \theta^2} + \frac{\partial^2}{\partial z^2}.$$

The constitutive relations can be expressed as

$$\sigma_{ij} = 2Ge_{ij} + \frac{2G\nu}{1-2\nu}\delta_{ij}e_v - \alpha\delta_{ij}p, \quad (i,j=r,\theta,z), \tag{5}$$

$$p = -\frac{2GB(1+\nu_u)}{3(1-2\nu_u)}e_v - \frac{2GB^2(1-\nu)(1+\nu_u)^2}{9(\nu-\nu_u)(1-2\nu_u)}\varepsilon_v, \tag{6}$$

where σ_{ij} and e_{ij} are the total stress tension and strain tension, respectively;

$$\alpha = \frac{3(\nu_u - \nu)}{B(1 - 2\nu)(1 + \nu_u)}$$

is the Biot effective stress coefficient or the pore pressure coefficient (PPC); δ_{ij} is the Kronecker delta function; and p is the excess pore water pressure. Note that tension stress and compressive pore pressure are taken as positive in the present analysis.

3. Formulation of the problem

As shown schematically in Figure 1a, before drilling, the saturated medium is under in-situ compressive stress condition with the three principal stresses $S_{x'}$, $S_{y'}$, and $S_{z'}$ coinciding with the Cartesian coordinate system (x', y', z'). The initial pore pressure is assumed to be hydrostatic with a magnitude of p_0. Following the treatment by Cui et al. [1997] and Abousleiman and Nguyen [2005], a borehole local coordinate system (x, y, z), which is defined by a rotation of an azimuth angle $\varphi_{z'}$ about the z' axis and then by an inclination of a zenith angle φ_y towards the x-axis, is introduced for convenience of the solution presentation. The borehole axis is consistent with the z axis (Figure 1a). It is also assumed that the borehole is being pumped at a steady rate Q_0 (l/min) over a finite length $2b$.

The six components of the far-field stress tensor in the local coordinate system, S_x, S_y, S_z, S_{xy}, S_{yz}, and S_{xz} (See Figure 1b, where r and θ are the polar coordinates), are readily obtainable from the three principal stresses via a transformation matrix [Jaeger and Cook 1969]. So the stress boundary conditions at the far field ($r \to \infty$), under the local coordinate system, can be written as

$$\sigma_{xx} = -S_x, \quad \sigma_{yy} = -S_y, \quad \sigma_{zz} = -S_z, \quad \sigma_{xy} = -S_{xy}, \quad \sigma_{yz} = -S_{yz}, \quad \sigma_{xz} = -S_{xz}, \quad p = p_0. \quad (7)$$

While on the surface of the wellbore, $r = R$,

$$\sigma_{rr} = \begin{cases} -p & 0 \le |z| \le b, \\ 0 & b < |z| < \infty, \end{cases} \tag{8a}$$

$$\sigma_{r\theta} = 0, \tag{8b}$$

$$\sigma_{rz} = 0, \tag{8c}$$

$$q = \begin{cases} Q_0/4\pi Rb & 0 \le |z| \le b, \\ 0 & b < |z| < \infty, \end{cases} \tag{8d}$$

where $q = -\kappa \, dp/dr$ is the fluid flow rate in units of cm/min. Note that in [Rajapakse 1993], instead of (8a), a simpler but incorrect boundary condition for radial stress at the borehole wall was adopted ($\sigma_{rr} = 0$ for $|z| \le \infty$).

Equation (8d) identifies a flow boundary condition that the borehole is drilled with an impermeable casing but perforated over a length of $2b$ for fluid injection, a commonly encountered case in drilling practice. It must be noted that in the above the far field boundary conditions are expressed in the Cartesian coordinates, but at the borehole surface the polar coordinates are used for convenience.

Combining the governing equations (1)–(6) and boundary conditions (7)–(8) fully defines the concerned problem of an inclined borehole subjected to in-situ stresses and fluid loading. To simplify the

analysis it is better to employ the superposition method and decompose the problem into two fundamental parts, solving (1)–(6) separately with the incorporation of the following two boundary conditions:

I: Fluid discharge problem. In the far field ($r \to \infty$),

$$\sigma_{xx} = \sigma_{yy} = \sigma_{zz} = \sigma_{xy} = \sigma_{yz} = \sigma_{xz} = p = 0. \tag{9}$$

At the borehole wall ($r = R$),

$$\sigma_{r\theta} = \sigma_{rz} = 0, \qquad \sigma_{rr} = \begin{cases} -p & 0 \le |z| \le b, \\ 0 & b < |z| < \infty, \end{cases} \qquad q = \begin{cases} Q_0/4\pi Rb & 0 \le |z| \le b, \\ 0 & b < |z| < \infty. \end{cases} \tag{10}$$

II: Stress boundary problem. In the far field ($r \to \infty$),

$$\sigma_{xx} = -S_x, \quad \sigma_{yy} = -S_y, \quad \sigma_{zz} = -S_z, \quad \sigma_{xy} = -S_{xy}, \quad \sigma_{yz} = -S_{yz}, \quad \sigma_{xz} = -S_{xz}, \quad p = p_0. \tag{11}$$

At the borehole wall ($r = R$),

$$\sigma_{rr} = \begin{cases} -p & \text{if } |z| \le b, \\ 0 & \text{if } |z| > b, \end{cases} \qquad \sigma_{r\theta} = 0, \qquad \sigma_{rz} = 0, \qquad q = 0. \tag{12}$$

Figures 1c–1d illustrate the detailed decomposition scheme. It is obviously observed that after the addition of (9)–(12) the original boundary equations (7)–(8) are identically recovered.

4. Solutions for fundamental problems

The decomposition methodology demonstrated above enables us to find the solutions of individual problems and subsequently superpose the results yielding the final solution. Among them, problem I can be treated using the conventional integral transform technique, while the solutions of problem II will be approximated by directly employing the results of Cui et al. [1998] for an impermeable wellbore problem.

I: Fluid discharge problem. This problem is axially symmetric (all quantities independent of θ), so Equations (1)–(6) can be simplified as follows:

$$\frac{\partial^2 u_r^{(I)}}{\partial r^2} + \frac{1}{r}\frac{\partial u_r^{(I)}}{\partial r} - \frac{u_r^{(I)}}{r^2} + \frac{\partial^2 u_r^{(I)}}{\partial z^2} + \frac{1}{1-2\nu_u}\frac{\partial e_v^{(I)}}{\partial r} - \frac{2B(1+\nu_u)}{3(1-2\nu_u)}\frac{\partial \varepsilon_v^{(I)}}{\partial r} = 0, \tag{13}$$

$$\frac{\partial^2 u_z^{(I)}}{\partial r^2} + \frac{1}{r}\frac{\partial u_z^{(I)}}{\partial r} + \frac{\partial^2 u_z^{(I)}}{\partial z^2} + \frac{1}{1-2\nu_u}\frac{\partial e_v^{(I)}}{\partial z} - \frac{2B(1+\nu_u)}{3(1-2\nu_u)}\frac{\partial \varepsilon_v^{(I)}}{\partial z} = 0, \tag{14}$$

$$\frac{\partial^2 \varepsilon_v^{(I)}}{\partial r^2} + \frac{1}{r}\frac{\partial \varepsilon_v^{(I)}}{\partial r} + \frac{\partial^2 \varepsilon_v^{(I)}}{\partial z^2} = \frac{1}{c}\frac{\partial \varepsilon_v^{(I)}}{\partial t}, \tag{15}$$

$$p^{(I)} = -\frac{2GB(1+\nu_u)}{3(1-2\nu_u)}e_v^{(I)} - \frac{2GB^2(1-\nu)(1+\nu_u)^2}{9(\nu-\nu_u)(1-2\nu_u)}\varepsilon_v^{(I)}, \tag{16}$$

$$\sigma_{rr}^{(I)} = 2G\frac{\partial u_r^{(I)}}{\partial r} + \frac{2G\nu}{1-2\nu}e_v^{(I)} - \frac{3(\nu_u-\nu)}{B(1-2\nu)(1+\nu_u)}p^{(I)}, \tag{17}$$

$$\sigma_{zz}^{(I)} = 2G\frac{\partial u_z^{(I)}}{\partial z} + \frac{2Gv}{1-2v}e_v^{(I)} - \frac{3(v_u - v)}{B(1-2v)(1+v_u)}p^{(I)}, \tag{18}$$

$$\sigma_{\theta\theta}^{(I)} = 2G\frac{u_r^{(I)}}{r} + \frac{2Gv}{1-2v}e_v^{(I)} - \frac{3(v_u - v)}{B(1-2v)(1+v_u)}p^{(I)}, \tag{19}$$

$$\sigma_{rz}^{(I)} = G\left[\frac{\partial u_r^{(I)}}{\partial z} + \frac{\partial u_z^{(I)}}{\partial r}\right], \tag{20}$$

$$u_\theta^{(I)} = \sigma_{r\theta}^{(I)} = \sigma_{\theta z}^{(I)} = 0, \tag{21}$$

where the superscript (I) is added to distinguish the displacement and stress components for the first problem (fluid discharge) from those corresponding to problem II (stress boundary).

Introduce the Laplace and Fourier integral transforms with respect to t and z coordinates

$$\tilde{f}(r, z, s) = \int_0^\infty f(r, z, t)e^{-st}\, dt, \qquad f(r, z, t) = \frac{1}{2\pi i}\int_{\gamma-i\infty}^{\gamma+i\infty}\tilde{f}(r, z, s)e^{st}\, ds, \tag{22}$$

$$\hat{f}(r, \xi, t) = \frac{1}{\sqrt{2\pi}}\int_{-\infty}^\infty f(r, z, t)e^{i\xi z}\, dz, \qquad f(r, z, t) = \frac{1}{\sqrt{2\pi}}\int_{-\infty}^\infty \hat{f}(r, \xi, t)e^{-i\xi z}\, d\xi, \tag{23}$$

where s and ξ are parameters for the Laplace and Fourier transforms, respectively, and γ is greater than the real part of all singularities of $\tilde{f}(r, z, s)$.

Equation (15) becomes, after Laplace and Fourier transformations,

$$\left[\frac{d^2}{dr^2} + \frac{1}{r}\frac{d}{dr} - \left(\xi^2 + \frac{s}{c}\right)\right]\hat{\tilde{\varepsilon}}_v^{(I)} = 0, \tag{24}$$

which has the solution

$$\hat{\tilde{\varepsilon}}_v^{(I)} = A(\xi, s)K_0(\eta r), \tag{25}$$

where $\eta = +\sqrt{\xi^2 + s/c}$ and $A(\xi, s)$ is an arbitrary function of ξ and s.

Application of the transforms to (13) and (14) results in

$$\left(\frac{d^2}{dr^2} + \frac{1}{r}\frac{d}{dr} - \xi^2\right)\hat{\tilde{e}}_v^{(I)} = \frac{B(1+v_u)}{3(1-v_u)}\left(\frac{d^2}{dr^2} + \frac{1}{r}\frac{d}{dr} - \xi^2\right)\hat{\tilde{\varepsilon}}_v^{(I)}. \tag{26}$$

It then follows from (25) and (26) that

$$\hat{\tilde{e}}_v^{(I)} = C(\xi, s)|\xi|K_0(\rho) + \frac{B(1+v_u)}{3(1-v_u)}A(\xi, s)K_0(\eta r), \tag{27}$$

where $\rho = |\xi|r$ and $C(\xi, s)$ is another arbitrary function of ξ and s. The pore pressure can thus be obtained by back substitution of (25) and (27) into the Laplace and Fourier transforms of (16), yielding

$$\hat{\tilde{p}}^{(I)} = -\frac{2GB^2(1-v)(1+v_u)^2}{9(v-v_u)(1-v_u)}K_0(\eta r)A(\xi, s) - \frac{2GB(1+v_u)}{3(1-2v_u)}|\xi|K_0(\rho)C(\xi, s) \tag{28}$$

and hence

$$\hat{\tilde{q}}^{(I)} = -\kappa\frac{d\hat{\tilde{p}}^{(I)}}{dr} = -\frac{2GB^2(1-v)(1+v_u)^2}{9(v-v_u)(1-v_u)}\eta K_1(\eta r)A(\xi, s) - \frac{2G\kappa B(1+v_u)}{3(1-2v_u)}\xi^2 K_1(\rho)C(\xi, s). \tag{29}$$

Similarly, by substituting (25) and (27) into (13) and (14), one has for the displacement components

$$\left(\frac{d^2}{dr^2} + \frac{1}{r}\frac{d}{dr} - \frac{1}{r^2} - \xi^2\right)\hat{\tilde{u}}_r^{(I)} = -\frac{B(1+\nu_u)}{3(1-\nu_u)}\eta K_1(\eta r)A(\xi,s) + \frac{\xi^2 K_1(\rho)}{1-2\nu_u}C(\xi,s), \quad (30)$$

$$\left(\frac{d^2}{dr^2} + \frac{1}{r}\frac{d}{dr} - \xi^2\right)\hat{\tilde{u}}_z^{(I)} = -\frac{i\xi B(1+\nu_u)}{3(1-\nu_u)}K_0(\eta r)A(\xi,s) + \frac{i\xi|\xi|K_0(\rho)}{1-2\nu_u}C(\xi,s), \quad (31)$$

and the resulting solutions are

$$\hat{\tilde{u}}_r^{(I)} = -\frac{B(1+\nu_u)\eta c}{3(1-\nu_u)s}K_1(\eta r)A(\xi,s) - \left(K_1(\rho) + \frac{\rho K_2(\rho)}{2(1-2\nu_u)}\right)C(\xi,s) - i\xi K_1(\rho)D(\xi,s), \quad (32)$$

$$\hat{\tilde{u}}_z^{(I)} = -\frac{i\xi B(1+\nu_u)c}{3(1-\nu_u)s}K_0(\eta r)A(\xi,s) - \frac{i\xi r}{2(1-2\nu_u)}K_1(\rho)C(\xi,s) + |\xi|K_0(\rho)D(\xi,s), \quad (33)$$

where $D(\xi,s)$ is again an arbitrary function of ξ and s.

Finally, it is not difficult to derive the stress expressions from (17)–(20) as follows:

$$\frac{\hat{\tilde{\sigma}}_{rr}^{(I)}}{2G} = \frac{B(1+\nu_u)}{3(1-\nu_u)}\left\{\left(\frac{c\eta^2}{s} - 1\right)K_0(\eta r) + \frac{c\eta}{sr}K_1(\eta r)\right\}A(\xi,s) + i\xi\left\{|\xi|K_0(\rho) + \frac{K_1(\rho)}{r}\right\}D(\xi,s)$$
$$+ \left\{\frac{1-\nu_u}{1-2\nu_u}|\xi|K_0(\rho) + \left(\frac{1}{r} + \frac{\rho|\xi|}{2(1-2\nu_u)}\right)K_1(\rho) + \frac{|\xi|}{2(1-2\nu_u)}K_2(\rho)\right\}C(\xi,s), \quad (34)$$

$$\frac{\hat{\tilde{\sigma}}_{zz}^{(I)}}{2G} = \frac{B(1+\nu_u)}{3(1-\nu_u)}\left(-\frac{c\xi^2}{s} - 1\right)K_0(\eta r)A(\xi,s)$$
$$+ \left\{\frac{\nu_u}{1-2\nu_u}|\xi|K_0(\rho) - \frac{\xi^2 r}{2(1-2\nu_u)}K_1(\rho)\right\}C(\xi,s) - i\xi|\xi|K_0(\rho)D(\xi,s), \quad (35)$$

$$\frac{\hat{\tilde{\sigma}}_{\theta\theta}^{(I)}}{2G} = \frac{B(1+\nu_u)}{3(1-\nu_u)}\left(-K_0(\eta r) - \frac{c\eta}{sr}K_1(\eta r)\right)A(\xi,s)$$
$$+ \left\{\frac{\nu_u}{1-2\nu_u}|\xi|K_0(\rho) - \frac{K_1(\rho)}{r} - \frac{|\xi|}{2(1-2\nu_u)}K_2(\rho)\right\}C(\xi,s) - i\frac{\xi}{r}K_1(\rho)D(\xi,s), \quad (36)$$

$$\frac{\hat{\tilde{\sigma}}_{rz}^{(I)}}{2G} = \frac{i\xi B(1+\nu_u)c}{3(1-\nu_u)s}\eta K_1(\eta r)A(\xi,s)$$
$$+ \left\{\frac{i\xi\rho}{4(1-2\nu_u)}(K_0(\rho) + K_2(\rho)) + \frac{i\xi}{2}K_1(\rho)\right\}C(\xi,s) - \xi^2 K_1(\rho)D(\xi,s). \quad (37)$$

In deriving these displacement and stress solutions, the far field boundary condition (9) has been already taken into account. The three unknown functions $A(\xi,s)$, $C(\xi,s)$, and $D(\xi,s)$ should be determined from the transformed versions of the boundary conditions (10), that is,

$$\hat{\tilde{\sigma}}_{rz}^{(I)}(R,\xi,s) = 0, \quad (38)$$

$$\frac{1}{\sqrt{2\pi}} \int_{-\infty}^{\infty} [\hat{\bar{\sigma}}_{rr}^{(I)}(R, \xi, s) + \hat{\bar{p}}^{(I)}(R, \xi, s)] e^{-i\xi z} \, d\xi = 0, \quad 0 \leq |z| \leq b,$$

$$\frac{1}{\sqrt{2\pi}} \int_{-\infty}^{\infty} \hat{\bar{\sigma}}_{rr}^{(I)}(R, \xi, s) e^{-i\xi z} \, d\xi = 0, \qquad\qquad b \leq |z| \leq \infty, \tag{39}$$

$$\hat{\bar{q}}^{(I)}(R, \xi, s) = \frac{\sin(\xi b)}{\sqrt{2\pi}\xi s} \frac{Q_0}{2\pi Rb} = \frac{2q_0 \sin(\xi b)}{\sqrt{2\pi}\xi s} = -\Omega(\xi, s), \tag{40}$$

where

$$q_0 = \frac{Q_0}{4\pi Rb} \quad \text{and} \quad \Omega(\xi, s) = -\frac{\sin(\xi b)}{\sqrt{2\pi}\xi s} \frac{Q_0}{2\pi Rb}.$$

On incorporating (29), (34), and (37) into (38) and (40), one can easily determine the three unknown functions in terms of $\hat{\bar{\sigma}}_{rr}^{(I)}(R, \xi, s)$ as follows:

$$A(\xi, s) = \frac{1}{\Delta} \left(-\alpha_{23}\alpha_{32} \hat{\bar{\sigma}}_{rr}^{(I)}(R, \xi, s) + (\alpha_{12}\alpha_{23} - \alpha_{22}\alpha_{13})\Omega(\xi, s) \right), \tag{41}$$

$$C(\xi, s) = \frac{1}{\Delta} \left(\alpha_{23}\alpha_{31} \hat{\bar{\sigma}}_{rr}^{(I)}(R, \xi, s) + (\alpha_{21}\alpha_{13} - \alpha_{11}\alpha_{23})\Omega(\xi, s) \right), \tag{42}$$

$$D(\xi, s) = \frac{1}{\Delta} \left((\alpha_{21}\alpha_{32} - \alpha_{31}\alpha_{22}) \hat{\bar{\sigma}}_{rr}^{(I)}(R, \xi, s) + (\alpha_{11}\alpha_{22} - \alpha_{21}\alpha_{12})\Omega(\xi, s) \right), \tag{43}$$

where $\Delta = \alpha_{12}\alpha_{23}\alpha_{31} + \alpha_{13}\alpha_{21}\alpha_{32} - \alpha_{11}\alpha_{23}\alpha_{32} - \alpha_{13}\alpha_{22}\alpha_{31}$ and

$$\alpha_{11} = 2G\frac{B(1+\nu_u)}{3(1-\nu_u)} \left\{ \left(\frac{c\eta^2}{s} - 1 \right) K_0(\eta R) + \frac{c\eta}{sR} K_1(\eta R) \right\},$$

$$\alpha_{12} = 2G \left\{ \frac{1-\nu_u}{1-2\nu_u} |\xi| K_0(|\xi|R) + \left[\frac{1}{R} + \frac{\xi^2 R}{2(1-2\nu_u)} \right] K_1(|\xi|R) + \frac{|\xi|}{2(1-2\nu_u)} K_2(|\xi|R) \right\},$$

$$\alpha_{13} = 2Gi\xi \left\{ |\xi| K_0(|\xi|R) + \frac{K_1(|\xi|R)}{R} \right\}, \qquad \alpha_{21} = 2G\frac{i\xi B(1+\nu_u)c}{3(1-\nu_u)s} \eta K_1(\eta R),$$

$$\alpha_{22} = 2G \left\{ \frac{i\xi |\xi| R}{4(1-2\nu_u)} [K_0(|\xi|R) + K_2(|\xi|R)] + \frac{i\xi}{2} K_1(|\xi|R) \right\}, \qquad \alpha_{23} = -2G\xi^2 K_1(|\xi|R),$$

$$\alpha_{31} = \frac{2G\kappa B^2(1-\nu)(1+\nu_u)^2}{9(\nu-\nu_u)(1-2\nu_u)} \eta K_1(\eta R), \qquad \alpha_{32} = \frac{2G\kappa B(1+\nu_u)}{3(1-2\nu_u)} \xi^2 K_1(|\xi|R).$$

It is obvious that if $\hat{\bar{\sigma}}_{rr}^{(I)}(R, \xi, s) = 0$, which is the case in [Rajapakse 1993], $A(\xi, s)$, $C(\xi, s)$, and $D(\xi, s)$ can be expressed in explicit form with $\Omega(\xi, s)$. However, for the current boundary conditions where $\hat{\bar{\sigma}}_{rr}^{(I)}(R, \xi, s) \neq 0$, one has to seek the numerical solutions of these three unknown functions, as discussed below.

Substituting (41) and (42) into (28), one has

$$\hat{\bar{p}}^{(I)}(R, \xi, s) = f_1(\xi, s)\hat{\bar{\sigma}}_{rr}^{(I)}(R, \xi, s) + f_2(\xi, s)\Omega(\xi, s), \tag{44}$$

where

$$f_1(\xi, s) = \frac{1}{\Delta}(-\alpha_{23}\alpha_{32}\alpha_{31p} + \alpha_{23}\alpha_{31}\alpha_{32p}),$$

$$f_2(\xi, s) = \frac{1}{\Delta}\big((\alpha_{21}\alpha_{13} - \alpha_{11}\alpha_{23})\alpha_{32p} + (\alpha_{12}\alpha_{23} - \alpha_{22}\alpha_{13})\alpha_{31p}\big)$$

with

$$\alpha_{31p} = -\frac{2GB^2(1-\nu)(1+\nu_u)^2}{9(\nu - \nu_u)(1-\nu_u)}K_0(\eta R), \qquad \alpha_{32p} = -\frac{2GB(1+\nu_u)}{3(1-2\nu_u)}|\xi|K_0(|\xi|R).$$

Now the boundary condition (39), combined with (44), can be transformed into the following dual integral equations

$$\int_{-\infty}^{\infty}[1 + f_1(\xi, s)]\hat{\bar{\sigma}}_{rr}^{(I)}(R, \xi, s)e^{-i\xi z}d\xi = -\int_{-\infty}^{\infty} f_2(\xi, s)\Omega(\xi, s)e^{-i\xi z}\,d\xi, \quad 0 \le |z| \le b,$$

$$\int_{-\infty}^{\infty} \hat{\bar{\sigma}}_{rr}^{(I)}(R, \xi, s)e^{-i\xi z}\,d\xi = 0, \qquad\qquad\qquad b < |z| < \infty. \tag{45}$$

It is found that $f_1(\xi, s)$, $f_2(\xi, s)$, and $\hat{\bar{\sigma}}_{rr}^{(I)}(R, \xi, s)$ are all real even functions of ξ, so the above dual integral equations can be further simplified as

$$\int_0^{\infty} \xi^{1/2}[1 + f_1(\xi, s)]\,\hat{\bar{\sigma}}_{rr}^{(I)}(R, \xi, s)J_{-1/2}(\xi z)\,d\xi = \sqrt{\frac{2}{\pi z}}g(z, s), \qquad 0 \le z \le b,$$

$$\int_0^{\infty} \xi^{1/2}\hat{\bar{\sigma}}_{rr}^{(I)}(R, \xi, s)J_{-1/2}(\xi z)\,d\xi = 0, \qquad\qquad b < z < \infty, \tag{46}$$

where

$$g(z, s) = -\int_0^{\infty} f_2(\xi, s)\Omega(\xi, s)\cos(\xi z)\,d\xi \tag{47}$$

and $\lim_{\xi \to \infty} f_1(\xi, s) = 0$. Introducing the function $\theta(x, s)$ by [Noble 1963]

$$\hat{\bar{\sigma}}_{rr}^{(I)}(R, \xi, s) = \frac{2}{\pi}\int_0^b \theta(x, s)\cos(x\xi)\,dx; \tag{48}$$

equations (46) are equivalent to the following Fredholm integral equation of the second kind

$$\theta(x, s) + \frac{2}{\pi}\int_0^b M(x, y, s)\theta(y, s)\,dy = g(x, s), \tag{49}$$

where

$$M(x, y, s) = \int_0^{\infty} f_1(\xi, s)\cos(x\xi)\cos(y\xi)d\xi. \tag{50}$$

Equations (48)–(50) determine $\hat{\bar{\sigma}}_{rr}^{(I)}(R, \xi, s)$ in the Laplace–Fourier transformed domain, and the three unknown functions $A(\xi, s)$, $C(\xi, s)$, and $D(\xi, s)$ can thus be numerically obtained from (41)–(43). Once $A(\xi, s)$, $C(\xi, s)$, and $D(\xi, s)$ are known, one can obtain the final solutions for the physical quantities such as displacement and stress components of the solid matrix, pore water pressure, and fluid discharge through the inversion of Laplace and Fourier transforms. It is important to note that $A(\xi, s)$, $C(\xi, s)$, and Δ are real even functions of ξ while $D(\xi, s)$ a pure imaginary odd function of ξ, the infinite integrals for the inverse Fourier transforms are thus reduced to the evaluation of a semiinfinite integral.

Note that the plane strain problem can be obtained by keeping the fluid flow rate $q_0 = Q_0/(4\pi R b)$ constant but allowing $b \to \infty$. As b approaches infinity, all the quantities with respect to z vanish. The fluid discharge problem for the borehole is thus governed only by (13) and (15). In this case the Fourier transform become redundant and it is found that the solutions can be solved directly in the Laplace domain as follows, where we have introduced $\tau = \sqrt{s/c}$:

$$\tilde{p}^{(I)} = \frac{K_0(r\tau)q_0}{s\kappa\tau K_1(R\tau)}, \tag{51}$$

$$\tilde{u}_r^{(I)} = \frac{q_0}{2G\kappa\tau K_1(R\tau)r}\left(R^2 K_0(R\tau) + \frac{\alpha(1-2\nu)}{1-\nu}\frac{RK_1(R\tau) - rK_1(r\tau)}{\tau}\right), \tag{52}$$

$$\tilde{\sigma}_{rr}^{(I)} = -\frac{q_0}{s\kappa\tau K_1(R\tau)r^2}\left(R^2 K_0(R\tau) + \frac{\alpha(1-2\nu)}{1-\nu}\frac{RK_1(R\tau) - rK_1(r\tau)}{\tau}\right), \tag{53}$$

$$\tilde{\sigma}_{\theta\theta}^{(I)} = \frac{q_0}{s\kappa\tau K_1(R\tau)}\left\{\frac{R^2}{r^2}K_0(R\tau) + \frac{\alpha(1-2\nu)}{1-\nu}\left(\frac{RK_1(R\tau)}{r^2\tau} - \frac{K_1(r\tau)}{r\tau} - K_0(r\tau)\right)\right\}. \tag{54}$$

II: Stress boundary problem. Since the pore pressure due to borehole drilling in case of an impermeable wall is much less than the pressure generated by the flux loading, the boundary condition for σ_{rr} can be modified to $\sigma_{rr} = 0$, without causing appreciable mathematical or applications errors. The modified boundary conditions at the borehole wall now correspond to a generalized plane stain problem. As first noted by Cui et al. [1997; 1998], such a problem can be subdivided further into three cases and the stress and pore pressure solutions, $\sigma_{rr}^{(II)}$, $\sigma_{\theta\theta}^{(II)}$, $\sigma_{zz}^{(II)}$, $\sigma_{r\theta}^{(II)}$, $\sigma_{rz}^{(II)}$, $\sigma_{\theta z}^{(II)}$, and $p^{(II)}$, may again be obtained using the principle of superposition. These solutions will not be repeated herein and the interested readers should refer to [Cui et al. 1997; 1998] for details.

5. Superposition

Once the stress solutions have been found for the two fundamental problems, the final solutions can be obtained by superposition based on these results, as formally shown below

$$\begin{aligned}
\sigma_{rr} = \sigma_{rr}^{(I)} + \sigma_{rr}^{(II)}, \quad \sigma_{\theta\theta} = \sigma_{\theta\theta}^{(I)} + \sigma_{\theta\theta}^{(II)}, \quad \sigma_{zz} = \sigma_{zz}^{(I)} + \sigma_{zz}^{(II)}, \\
\sigma_{r\theta} = \sigma_{r\theta}^{(II)}, \quad \sigma_{rz} = \sigma_{rz}^{(I)} + \sigma_{rz}^{(II)}, \quad \sigma_{\theta z} = \sigma_{\theta z}^{(II)}, \quad p = p^{(I)} + p^{(II)},
\end{aligned} \tag{55}$$

in which the trivial stress components are dropped.

6. Numerical schemes and comparisons

Due to the complexity of the integrands involved in conducting the Fourier and Laplace inversions, the stress components in the time domain corresponding to problems I and II have to be obtained numerically by applying approximate numerical schemes. As mentioned in the preceding section, the inverse Fourier transform arising from problem I turns to a semiinfinite integral which can be numerically integrated very accurately with Wolfram Mathematica 6.0, provided the upper limit of the integral is sufficiently large. In the ensuing numerical analyses, only the effective tangential stress and pore pressure will be
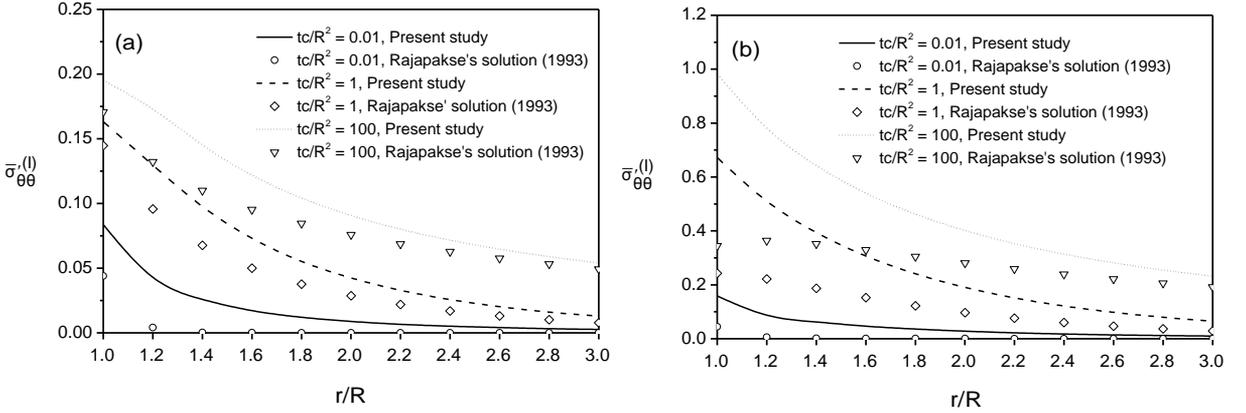
Figure 2. Comparison of effective tangential stress due to fluid injection over segment of length (a) $b/R = 0.25$; (b) $b/R = 1$.

considered as these are of critical importance to the study of borehole stability and fracturing, and the method of [Stehfest 1970] will be adopted in inverting the Laplace transform.

The Stehfest formula is

$$f(t) = \frac{\ln 2}{t} \sum_{n=1}^{N} X_n \tilde{f}\left(n\frac{\ln 2}{t}\right),\tag{56}$$

with the coefficient X_n given by

$$X_n = (-1)^{n+N/2} \sum_{j=\lfloor(n+1)/2\rfloor}^{\min(n,N/2)} \frac{j^{N/2}(2j)!}{(N/2-j)!j!(j-1)!(n-j)!(2j-n)!}.\tag{57}$$

The number of terms N in the series is even and a selection of $N = 8$ generally gives satisfactory results.

The errors caused by assuming a zero radial total stress at the borehole wall — that is, $\tilde{\sigma}_{rr}^{(I)}(R, z, t) = 0$ for $|z| \leq \infty$ — are tested by revisiting the fluid discharge problem of a borehole drilled in an infinite porous medium having incompressible constituents [Rajapakse 1993]. To make the comparison, the parameters $B = 0.999$, $\nu_u = 0.499$, $\nu = 0.3$ are adopted. Figure 2 shows the normalized effective tangential stress

$$\bar{\sigma}_{\theta\theta}^{'(I)} = \frac{\kappa\left[\sigma_{\theta\theta}^{(I)}(r, 0, tc/R^2) + p^{(I)}(r, 0, tc/R^2)\right]}{Rq_0}$$

versus the radial distance r/R for tc/R^2 ranging from 0.01 to 100 and for two values of b/R: 0.25 and 1. Although the two results exhibit a similar trend and the effective tangential stress is tensile along the radial distance, it is obvious that Rajapakse's solutions [1993] considerably underestimate the effective tangential stress near the borehole. This will accordingly lead to an overestimation of the fluid discharge needed to perform hydraulic fracturing.

7. Numerical results and discussions

We conducted some detailed parametric studies to examine the influence of permeability, borehole inclination, and the length of discharge loading on the stress distribution surrounding the borehole. To cover a wide range of permeabilities, three typical rocks, Ruhr sandstone, Danian chalk, and Gulf of

Rock type	G (MPa)	ν	ν_u	B	α	c (m²/day)	k (mD)
Ruhr sandstone	13000	0.12	0.3	0.849	0.645	424	0.2
Danian chalk	2200	0.227	0.354	0.709	0.725	3.67	0.01
Gulf of Mexico shale	760	0.219	0.447	0.868	0.968	0.0143	0.0001

Table 1. Poromechanics constants for various rocks.

Mexico shale [Abousleiman et al. 1996], are considered with their poromechanics properties listed in Table 1. In addition, the following parameters are adopted in the analysis: far field in-situ stress and pore pressure $S_{x'} = 20$ MPa, $S_{y'} = 18$ MPa, $S_{z'} = 25$ MPa, $p_0 = 9.8$ MPa, borehole radius $R = 0.1$ m, borehole rotation $\varphi_{z'} = 30°$, borehole inclination $\varphi_y = 60°$ (varying from $0°$ to $90°$ in investigating the influence of inclination), and unless otherwise stated, the fluid flow rate $Q_0 = 1.4$ l/min.

Figure 3 presents isochrones of the maximum effective tangential stress around the borehole (here $\max_{0 \le \theta \le 2\pi} \sigma'_{\theta\theta} = \sigma_{\theta\theta} + \alpha p$ occurs at the $\theta = -4.8°$ direction for the current in-situ stresses and borehole geometries involved) and the corresponding pore pressure against the radial distance at position $z = 0$, for the case of Ruhr sandstone. It is found that both the effective tangential stress and the pore pressure
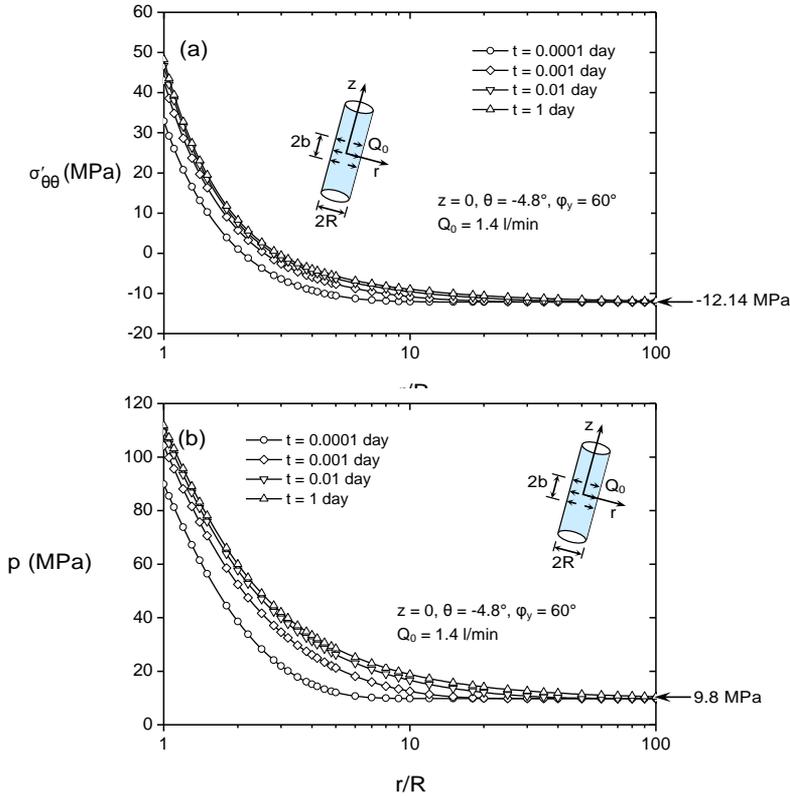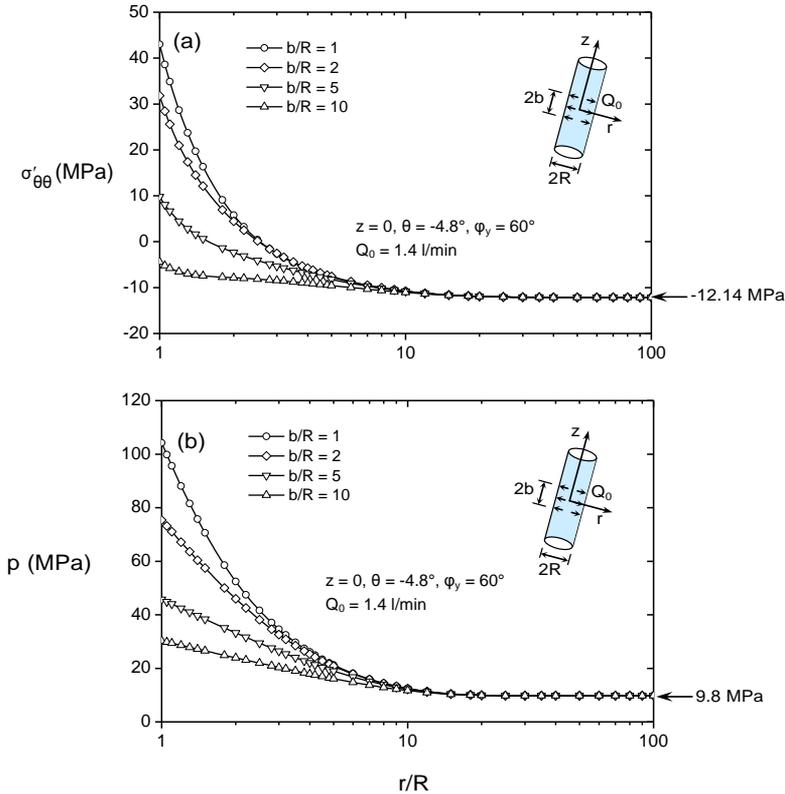

Figure 3. Isochrones of (top) maximum effective tangential stress and (bottom) pore pressure for Ruhr sandstone ($b/R = 1$).

generally increase as time progresses, deviating gradually from their in-situ values (It is recalled that positive values correspond to tension stress and compressive pore pressure, respectively). For all the time intervals considered, the induced pore pressures decrease monotonically as the radial distance increased, and fall uniformly to the virgin pore pressure $p_0 = 9.8\,\text{MPa}$. Notice that all the four pore pressure curves exhibit the same slope at the borehole wall as a direct consequence of the constant flux (q_0) boundary condition. It is also observed that the effective tangential stresses achieve their maximum values at the borehole wall and then gradually reduce to the in-situ compression stress of

$$\sigma'_{\theta\theta} = \tfrac{1}{2}(S_x + S_y) - \sqrt{S_{xy}^2 + \tfrac{1}{4}(S_x - S_y)^2} - \alpha p_0 = -12.14\,\text{MPa}$$

as r/R approaches infinity. This indicates that under the combined effects of borehole drilling and fluid flowing into the formation (The effective tangential stress attributed to the drilling of the borehole is compressive, while the fluid flowing into the borehole generates a tensile effective tangential stress), the tensile fracturing would most likely occur at the borehole wall and at a delayed time. This is not the case encountered in a purely drilling problem where the highest failure potential is usually located at some distance from the wellbore [Cui et al. 1997].

Figure 4 shows the influences of the discharge length b on the maximum effective tangential stress

Figure 4. Influences of discharge length on (top) maximum effective tangential stress and (bottom) pore pressure for Ruhr sandstone ($t = 0.001$ day).
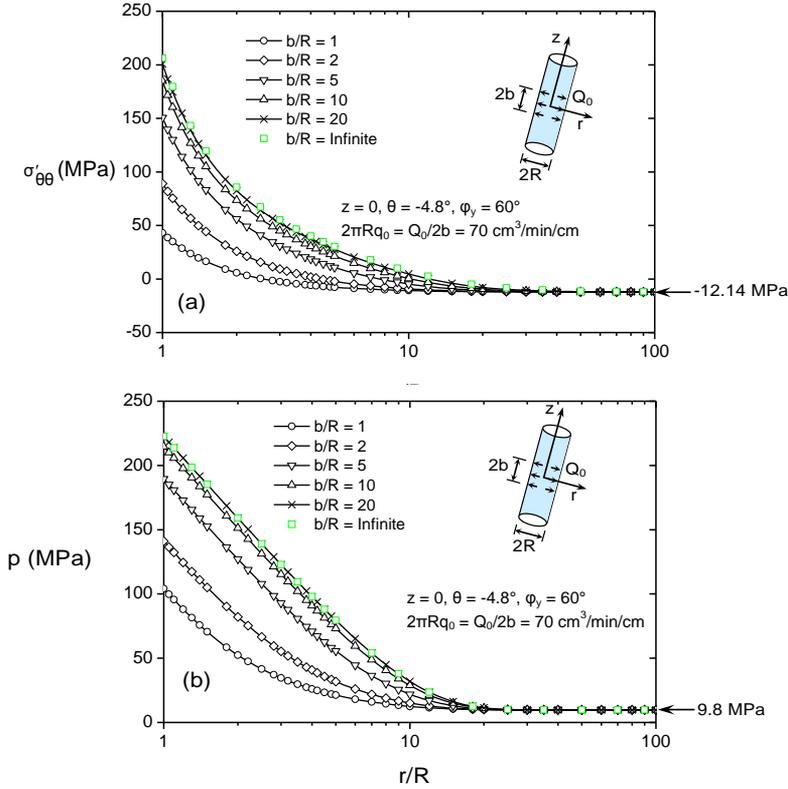
Figure 5. Variations of (top) maximum effective tangential stress and (bottom) pore pressure with discharge length for Ruhr sandstone in case of constant flow rate per unit length ($2\pi R q_0 = Q_0/2b = 70\,\text{cm}^3/\text{min/cm}$, $t = 0.001$ day).

and the pore pressure at $\theta = -4.8°$ direction for a specified time $t = 0.001$ day. It can be observed that both the effective tangential stress and the pore pressure generally decrease with the increasing discharge length. This is expected, because the fluid flow rate $q_0 = Q_0/(4\pi Rb)$ is inversely proportional to b which will lead to a reduced contribution of the tensile stress at $z = 0$ as b becomes larger, while the compressive effective tangential stress induced by the borehole opening, on the other hand, is independent of b. Indeed, the decrease in the flow rate q_0 due to increasing b has been clearly linked to the gradual slope drop of the pore pressure curves at $r/R = 1$. Figure 5 shows similar results for the maximum effective tangential stress and the pore pressure distributions at $\theta = -4.8°$ direction with varying discharge length b/R yet constant flow rate per unit length of $2\pi R q_0 = Q_0/2b = 70\,\text{cm}^3/\text{min/cm}$ (Q_0 in this case however becomes proportional to b/R). Also shown in this figure are the limiting plane strain solutions as $b \to \infty$ calculated directly from (51) and (54). It can be concluded from Figure 5 that the flux discharge length of $b/R = 10$ is sufficient large to approximate the planar flow conditions at the mid-section of the borehole.

To visualize variations of the effective tangential stress versus the whole range of the directional angle θ near the borehole drilled in Ruhr sandstone, Figures 6 and 7 present the contours of effective tangential stress at various inclination angles $\varphi_y = 0°$, $30°$, $60°$, and $90°$ and time intervals $t = 0.0001$, 0.001, 0.01, and 1 day, for $z = 0$ position and for the region of $1 \le r/R \le 5$. In these two figures the

x''-axis coincides with the direction of the minimum compressive principal in-situ stress in x-y plane and y'' with the maximum in-situ stress direction. Note that the angle between the x and the x'' axes, θ_r ($\theta_r = \frac{\pi}{2} + \arctan\frac{2S_{xy}}{S_x - S_y}$), varies with the inclination angle φ_y via S_{xy}, S_x, and S_y. For the four inclination angles changing from $0°$ to $90°$ (Figure 6), the resulting values of θ_r are found to be $60°$, $73.9°$, $85.2°$, and $90°$, respectively. As displayed in Figures 6 and 7, the stress distributions are symmetric with respect to the two principal in-situ stress directions, the highest value occurring along the y''-axis direction. When the inclination angle increases, the stress contours tend to rotate counterclockwise with the maximum effective tangential stress slightly increased from 40.7 MPa (Figure 6a) to 44.2 MPa (Figure 6d). For the four different times considered, however, the stress contours will retain almost the same shape, although from Figure 7a to 7d a steady increase in the maximum stress magnitude is clearly seen as time increases.
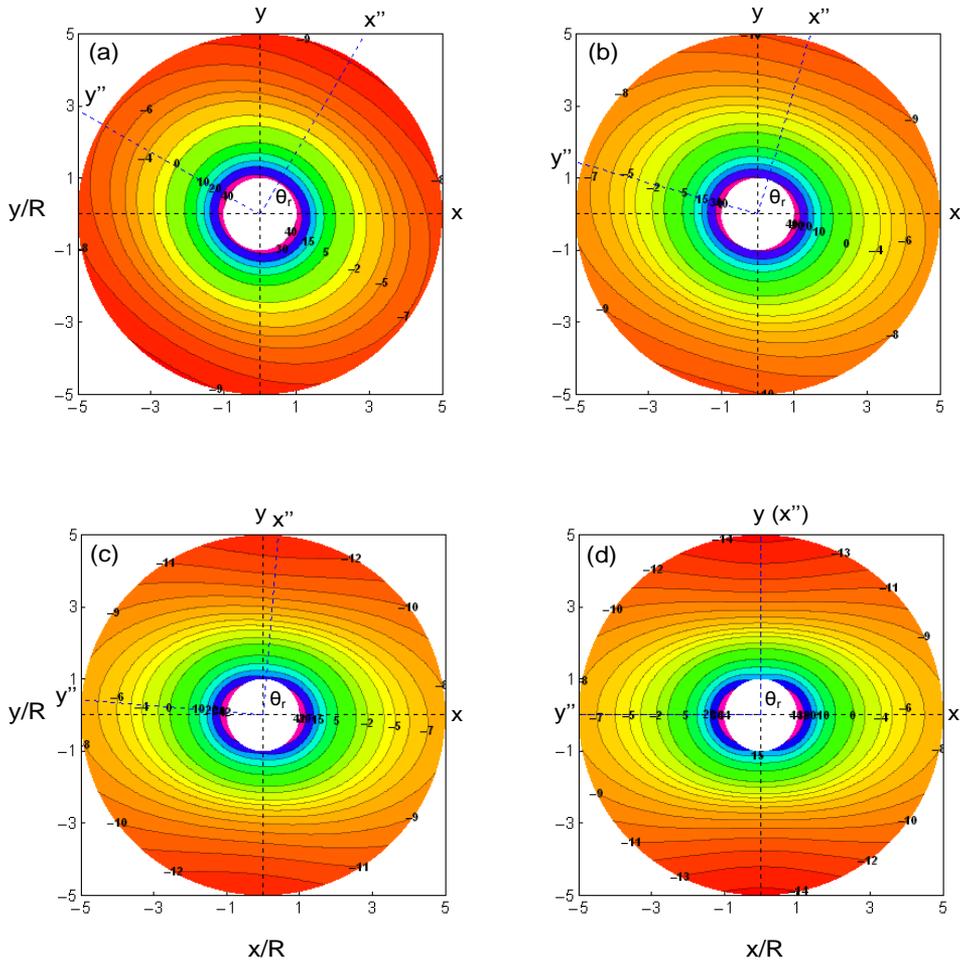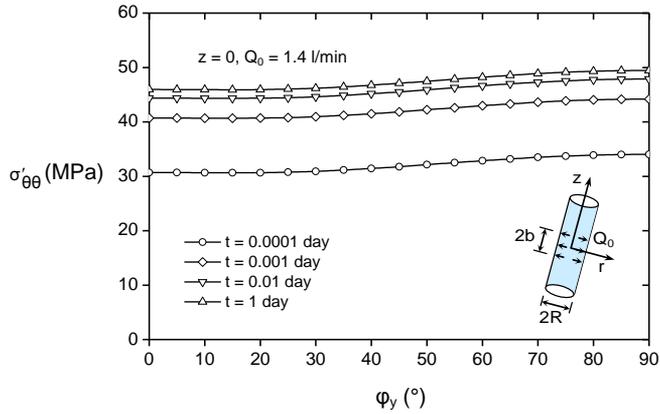

Figure 6. Effective tangential stress contours around the wellbore drilled in Ruhr sandstone with different inclination angles ($b/R = 1$, $t = 0.001$ day, $z = 0$, $1 \le r/R \le 5$): (a) $\varphi_y = 0°$, $\theta_r = 60°$; (b) $\varphi_y = 30°$, $\theta_r = 73.9°$; (c) $\varphi_y = 60°$, $\theta_r = 85.2°$; (d) $\varphi_y = 90°$, $\theta_r = 90°$.
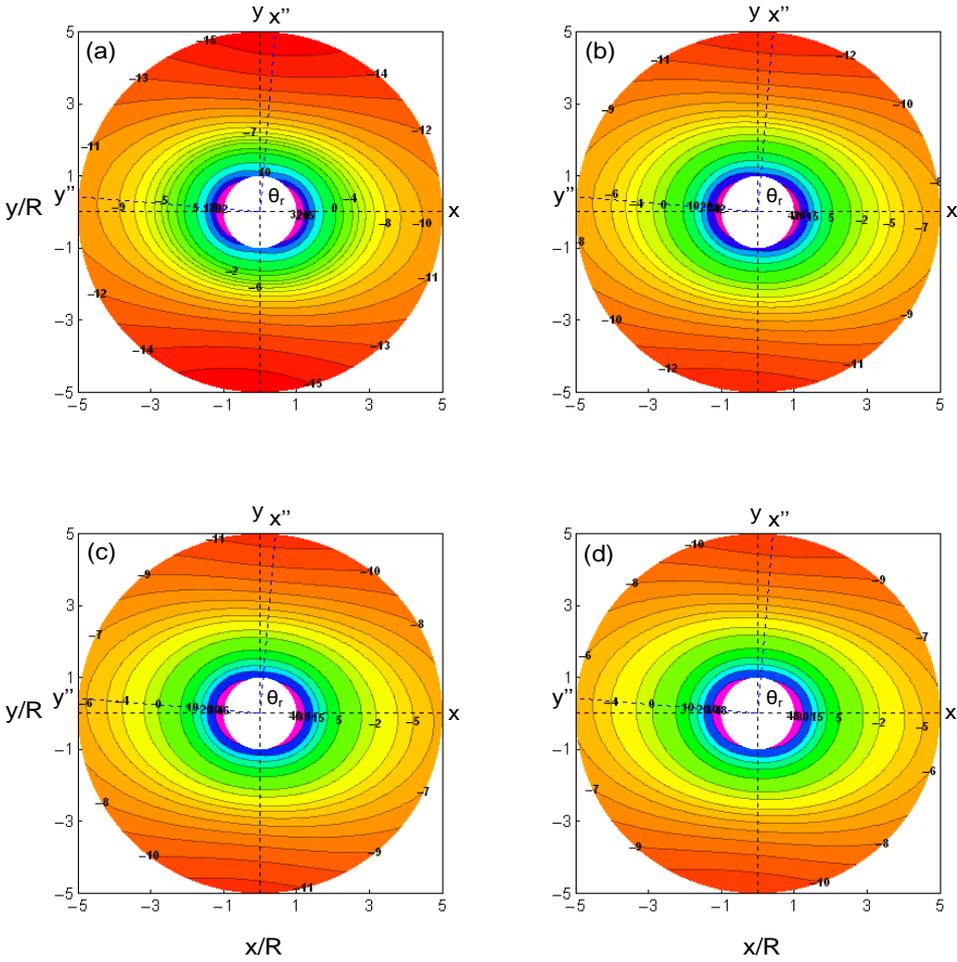
Figure 7. Effective tangential stress contours around the wellbore drilled in Ruhr sandstone at various times ($b/R = 1$, $\varphi_y = 60°$, $\theta_r = 85.2°$, $z = 0$, $1 \leq r/R \leq 5$): (a) $t = 0.0001$ day; (b) $t = 0.001$ day; (c) $t = 0.01$ day; (d) $t = 1$ day.

It is noteworthy that the flux induced effective tangential stress is independent with both φ_y and θ, thus the influences of these two parameters on the combined effective tangential stress are entered only through the stress term corresponding to the borehole drilling.

In Figure 8 the influence of the borehole inclination on the maximum effective tangential stress $\max_{0 \leq \theta \leq 2\pi} \sigma'_{\theta\theta}$, at the borehole wall and $z = 0$ position, are further illustrated for the Ruhr sandstone case. It is found that for all the time intervals, the variation of the maximum effective tangential stress with the inclination is somewhat complex and no longer monotonic. For small values of φ_y, an increase in the inclination angle is accompanied by a nearly indistinguishable reduction in the maximum effective tangential stress. As inclination reaches $\varphi_y = 20°$, however, the influence of the inclination becomes more noticeable and there is a tendency for the effective tangential stress to increase gradually with the inclination angle.
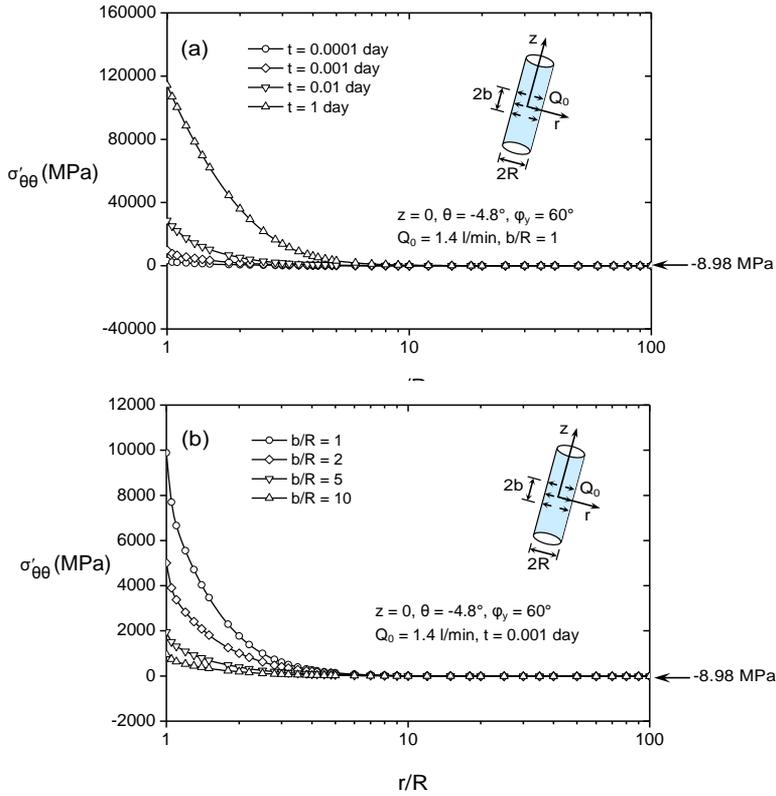
Figure 8. Variation of maximum effective tangential stress with borehole inclination for Ruhr sandstone ($b/R = 1, r/R = 1$).

Additionally, to see how the permeability of the saturated rock affects the stress behavior around the borehole, the solutions for Danian chalk and Gulf of Mexico shale are provided for $t = 0.0001, 0.001, 0.01$, and 1 day and $b/R = 1, 2, 5$, and 10, as plotted in Figures 9 and 10. In general, the influences of
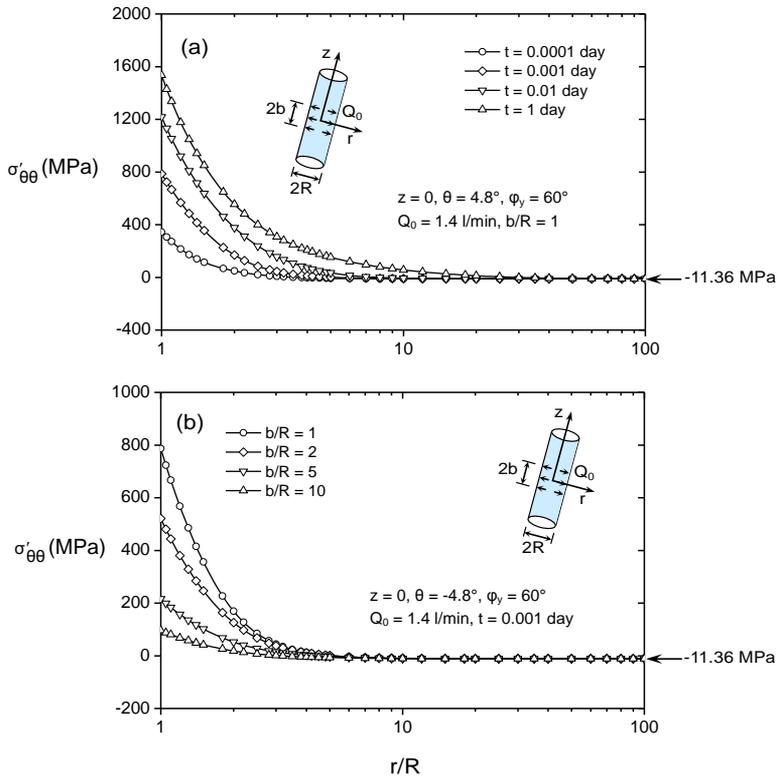
Figure 9. Variations of maximum effective tangential stress with radial distance at (top) various times and (bottom) various discharge length for Danian chalk.

Figure 10. Variations of maximum effective tangential stress with radial distance at (top) various times and (bottom) various discharge lengths for Gulf of Mexico shale.

the fluid discharge length and the time duration on the maximum effective tangential stress, which still occurs at $\theta = -4.8°$ direction for Danian chalk and Gulf of Mexico shale, are similar for the three rock formations with different permeabilities. However, when the permeability becomes smaller, say Danian chalk and Gulf of Mexico shale, the produced effective tangential stress under fixed fluid flow rate $Q_0 = 1.4$ l/min could be much greater and tend to level off much faster than in the relatively permeable formation like Ruhr sandstone. For example, in Figure 10 for Gulf of Mexico shale the predicted effective tangential stress may be as high as 120000 MPa. As in this case the effective tangential stress caused by the borehole drilling is maintained at a low level of around 20 MPa, very high effective tangential stress must be induced as a result of the fluid penetrating into the shale. This indicates that for low-permeable formations, the effective tangential stress is actually dominated by the flux loading. In reality, however, such large an effective tangential stress will never be reached since the tensile strength of a typical shale is less than 10 MPa.

Finally, it should be remarked that having known the stress distribution around a borehole, the analyses of the borehole fracturing will then become a simple matter. Moreover, the current solution can be employed to estimate the fluid flow rate that is required to trigger hydraulic fracturing, which will provide important guidance in the drilling practice.

8. Conclusions

An analytical method has been presented for the stress and pore pressure solutions of an inclined borehole subjected to the far-field three-dimensional in-situ stresses and to a fluid discharge applied over a finite segment of its surface. With the concept of superposition, the problem is decomposed into two fundamental parts whose solutions are simpler to handle. Comprehensive numerical analyses are also presented to examine the effects of some mechanical and geometrical parameters on the effective tangential stress and pore pressure distributions. The following conclusions are drawn:

(a) The existing solution for the limiting case of incompressible constituents which assumes a zero radial total stress along the whole wellbore surface tends to considerably underestimate the effective tangential stress near the borehole, which thus will lead to an overestimation of the fluid discharge needed to perform hydraulic fracturing.

(b) The effective tangential stress around a borehole subjected to a constant fluid flow rate generally increases with the time duration and with the decreasing loading length. The maximum effective tangential stress takes place at the borehole wall, which is not the case encountered in a purely drilling problem where the highest failure potential is usually located at some distance from the wellbore.

(c) The permeability has a pronounced influence on the predicted stress behavior. For a fixed fluid flow rate, the generated effective tangential stresses corresponding to highly impermeable Gulf of Mexico shale would be much greater and degrade much faster than those for Ruhr sandstone.

(d) In the particular case for Ruhr sandstone, the effective tangential stress distributions around the borehole are symmetric with respect to the two principal in-situ stress directions, the highest value occurring along the direction of the maximum compressive principal stress. An increase in the inclination angle φ_y has little influence on the estimated maximum effective tangential stress at the borehole wall for small values of φ_y, but will increase the maximum effective tangential stress and hence the possibility of a fracturing failure when φ_y exceeds $20°$.

(e) The present analysis can also be used to backfigure the fluid flow rate that is required to initiate a fracture around the borehole. This will provide important guidance in the drilling practice.

References

[Abousleiman and Ekbote 2005] Y. Abousleiman and S. Ekbote, "Solutions for the inclined borehole in a porothermoelastic transversely isotropic medium", *J. Appl. Mech.* (*ASME*) **72**:1 (2005), 102–114.

[Abousleiman and Nguyen 2005] Y. Abousleiman and V. Nguyen, "Poromechnanics response of inclined wellbore geometry in fractured porous media", *J. Eng. Mech.* (*ASCE*) **131**:11 (2005), 1170–1183.

[Abousleiman et al. 1996] Y. Abousleiman, A. H.-D. Cheng, C. Jiang, and J.-C. Roegiers, "Poroviscoelastic analysis of borehole and cylinder problems", *Acta Mech.* **119**:1–4 (1996), 199–219.

[Abousleiman et al. 1999] Y. Abousleiman, S. Ekbote, L. Cui, F. Mody, J.-C. Roegiers, and M. Zaman, "Time-dependent coupled processes in wellbore design and stability: PBORE-3D", in *SPE Annual Technical Conference and Exhibition* (Houston, TX, 1999), Society of Petroleum Engineers, Richardson, TX, 1999. Paper #56759-MS.

[Biot 1941] M. A. Biot, "General theory of three-dimensional consolidation", *J. Appl. Phys.* **12**:2 (1941), 155–164.

[Bowen 1982] R. M. Bowen, "Compressible porous media models by use of the theory of mixtures", *Int. J. Eng. Sci.* **20**:6 (1982), 697–735.

[Carter and Booker 1982] J. P. Carter and J. R. Booker, "Elastic consolidation around a deep circular tunnel", *Int. J. Solids Struct.* **18**:12 (1982), 1059–1074.

[Cui et al. 1997] L. Cui, A. H.-D. Cheng, and Y. Abousleiman, "Poroelastic solution for an inclined borehole", *J. Appl. Mech.* (*ASME*) **64**:1 (1997), 32–38.

[Cui et al. 1998] L. Cui, S. Ekbote, Y. Abousleiman, M. M. Zaman, and J.-C. Roegiers, "Borehole stability analyses in fluid saturated formations with impermeable walls", *Int. J. Rock Mech. Min. Sci.* **35**:4-5 (1998), 582–583.

[Cui et al. 1999] L. Cui, Y. Abouleiman, A. H.-D. Cheng, and J.-C. Roegiers, "Time-dependent failure analysis of inclined boreholes in fluid-saturated formations", *J. Energy Resour. Technol.* (*ASME*) **121**:1 (1999), 31–39.

[Detournay and Cheng 1988] E. Detournay and A. H.-D. Cheng, "Poroelastic response of a borehole in a non-hydrostatic stress field", *Int. J. Rock Mech. Min.* **25**:3 (1988), 171–182.

[Ekbote and Abousleiman 2005] S. Ekbote and Y. Abousleiman, "Porochemothermoelastic solution for an inclined borehole in a transversely isotropic formation", *J. Eng. Mech.* (*ASCE*) **131**:5 (2005), 522–533.

[Ekbote and Abousleiman 2006] S. Ekbote and Y. Abousleiman, "Porochemoelastic solution for an inclined borehole in a transversely isotropic formation", *J. Eng. Mech.* (*ASCE*) **132**:7 (2006), 754–763.

[Jaeger and Cook 1969] J. S. Jaeger and N. G. W. Cook, *Fundamentals of rock mechanics*, Chapman and Hall, New York, 1969.

[Noble 1963] B. Noble, "The solution of Bessel function dual integral equations by a multiplying-factor method", *Math. Proc. Cambridge Philos. Soc.* **59**:2 (1963), 351–362.

[Rajapakse 1993] R. K. N. D. Rajapakse, "Stress analysis of borehole in poroelastic medium", *J. Eng. Mech.* (*ASCE*) **119**:6 (1993), 1205–1227.

[Rice and Cleary 1976] J. R. Rice and M. P. Cleary, "Some basic stress diffusion solutions for fluid-saturated elastic porous media with compressible constituents", *Rev. Geophys.* **14**:2 (1976), 227–241.

[Stehfest 1970] H. Stehfest, "Algorithm 368: numerical inversion of Laplace transforms [D5]", *Commun. ACM* **13**:1 (1970), 47–49.

[Wang 2000] H. Wang, *Theory of poroelasticity with applications to geomechanics and hydrology*, Princeton University Press, Princeton, NJ, 2000.

YOUNANE N. ABOUSLEIMAN: yabousle@ou.edu
The University of Oklahoma, Poromechanics Institute, Mewbourne School of Petroleum & Geological Engineering, 100 East Boyd Street, Norman, OK 73019-1014, United States

SHENGLI CHEN: Shengli.Chen-1@ou.edu
The University of Oklahoma, Poromechanics Institute, Mewbourne School of Petroleum & Geological Engineering, 100 East Boyd Street, Norman, OK 73019-1014, United States